Measurement-Based Validation of Integrated Circuit Transient Electromagnetic Event Sensors

Shubhankar Marathe, *Member, IEEE*, Abhishek Patnaik, *Member, IEEE*, Rui Mi, Kaustav Ghosh, *Member, IEEE*, Jingook Kim, *Senior Member, IEEE*, David Pommerenke, *Fellow, IEEE*, and Daryl G. Beetner, *Senior Member, IEEE*

***Abstract*—Determining the components or coupling paths responsible for soft failures during transient testing is challenging because the components are hidden within the product and because measuring internal voltages or currents during a transient test may not be practical. Adding cables to make voltage or current measurements may be difficult and may alter the test results. To overcome this problem, in this article, two compact sensors are designed to measure the peak over or undervoltage on a trace or pin during a transient electromagnetic event. One sensor uses an analog-to-digital converter to store the peak voltage digitally and the other sensor uses an external capacitor to store an analog measure of the peak voltage for a period of time. The sensors are designed to wirelessly transmit the peak level to a remote receiver using the frequency-modulated electric and magnetic fields so that no cables or other changes to the system are needed. The proof-of-concept of the sensors was implemented in an integrated circuit using 180 nm technology. The sensor performance is characterized by direct injection and by using them to detect the peak voltage on a universal serial bus (USB) cable during a cable-guided transient event. Both sensors successfully detected and transmitted the peak level of the event.**

***Index Terms*—Electrostatic discharge (ESD), failure analysis, near-field probe, sensors, testing, transmission line pulser (TLP).**

Manuscript received December 15, 2019; revised May 26, 2020; accepted June 26, 2020. Date of publication July 15, 2020; date of current version August 13, 2020. This work was supported in part by the National Science Foundation under Grant IIP-1916535. This paper is for the Special Section and is an expanded version from the 2019 IEEE International Symposium on Electromagnetic Compatibility and Signal and Power Integrity in New Orleans. *(Corresponding author: Shubhankar Marathe.)*

Shubhankar Marathe was with the Electromagnetic Compatibility Laboratory, Missouri University of Science and Technology, Rolla, MO 65409 USA. He is now with the Amazon Lab126, Sunnyvale, CA 94089 USA (e-mail: skmcr4@mst.edu).

Abhishek Patnaik was with the Electromagnetic Compatibility Laboratory, Missouri University of Science and Technology, Rolla, MO 65409 USA. He is now with the Apple, Inc., Cupertino, CA 95014 USA (e-mail: ap437@mst.edu).

Rui Mi and Daryl G. Beetner are with the Electromagnetic Compatibility Laboratory, Missouri University of Science and Technology, Rolla, MO 65409 USA (e-mail: rmfd2@mst.edu; daryl@mst.edu).

Kaustav Ghosh was with the Electromagnetic Compatibility Laboratory, Missouri University of Science and Technology, Rolla, MO 65409 USA. He is now with the Juniper Networks, Inc., Sunnyvale, CA 94089 USA (e-mail: kgkb4@mst.edu).

Jingook Kim is with the School of Electrical and Computer Engineering, Ulsan National Institute of Science and Technology, Ulsan 689-798, South Korea (e-mail: jingook@unist.ac.kr).

David Pommerenke was with the Electromagnetic Compatibility Laboratory, Missouri University of Science and Technology, Rolla, MO 65409 USA. He is now with the University of Graz, 8036 Graz, Austria (e-mail: david.pommerenke@ieee.org).

Color versions of one or more of the figures in this article are available online at https://ieeexplore.ieee.org.

Digital Object Identifier 10.1109/TEMC.2020.3006166

I. Introduction

The ROOT cause analysis of soft failures during electrostatic discharge (ESD) testing is challenging in part because of the difficulty of measuring voltages or currents inside a product under test. Even if there is a space to connect a probe, the added cables or modifications to the enclosure may change the test result. A small, inexpensive sensor that could measure information about the transient event at specific points inside the product and wirelessly transmit this information to the user, without significant modifications to the system, could substantially assist with the process of finding the mechanisms responsible for ESD issues [1].

A variety of sensors have previously been developed for integrated circuits (ICs), which provide information about transient events [2]–[10]. None of these sensors, however, offers wireless transmission of the event information. In [2], a fuse and diode were implemented in parallel with the on-die ESD protection. If the voltage across the ESD protection exceeded a limit, the fuse would melt and allow postmortum discovery of the event level. In [3]–[5], the on-die power supply noise generated by a transient event was used to detect the presence and level of the event. In [6], an on-die oscilloscope circuit was proposed to monitor the ESD noise pulses at the power supply or the signal line. It sampled the noise waveform and converted the sampled digital data back to analog by postprocessing the data. In [7], the level of an event at an input/output (I/O) pin was determined by charging a capacitor connected to the pin through a diode and then measuring the charge on the capacitor. The designs in [8]–[10] integrated sensors into the I/O of a microcontroller to determine the presence, polarity, and level of the event. These sensors could be helpful for debugging soft errors, but the product must already use a microcontroller, which has these sensors embedded within it to be useful.

Sensors specifically designed to be added to a product during the debugging process were proposed in [11]. Two sensors were proposed, one using a simple analog-to-digital (A/D) converter to store a digital representation of the peak and another that stores a measure of the peak level of an event on an external capacitor. The sensors can wirelessly transmit information about the peak to a nearby electric- or magnetic-field probe by modulating the electric and magnetic fields at a frequency corresponding to the stored level.

The following article experimentally validates the sensor performance, which was only characterized by simulation in

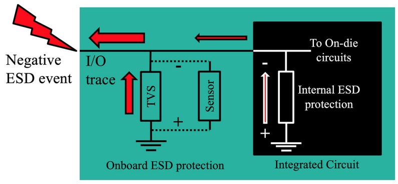

Fig. 1. Example connection of the sensor to a trace on a PCB. The arrows represent the direction of the current flow.

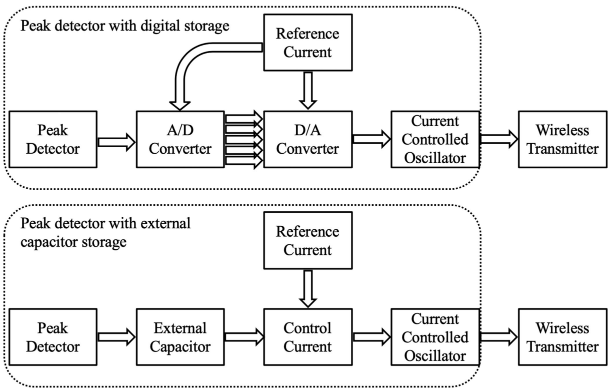

Fig. 2. Block diagrams of the A/D-based sensor (top) and of the sensor using an external storage capacitor (bottom).

[11]. The article is an extension of [12], which included limited experimental validation of the A/D-based sensor design. The results of characterizing the analog sensor utilizing an external capacitor are reported here, and the performance of the two designs is compared. Both sensors can only sense negative events, but this capability should be sufficient to demonstrate a proof-of-concept of the sensor designs. The sensors were first characterized by directly injecting a transient event to the sensor from a transmission line pulser (TLP) to their sense pin and were then used to determine the peak transient level seen on a universal serial bus (USB) signal line during a transient discharge to the enclosure of one of two products connected to the USB cable. Tests were also performed to demonstrate that the oscillating magnetic fields generated by the sensor could be measured outside of a typical enclosure and the level of the transient event determined.

II. Peak Transient Sensors

Fig. 1 shows the sensor placed on a trace connected to an IC and to a transient voltage suppressor (TVS). During a typical ESD event, the ESD current will be shared by the external TVS and by the internal (on-die) ESD protection circuitry. The proposed sensor was designed to measure the voltage on the trace while drawing minimal ESD current. Since the majority of ESD current typically flows through the TVS device, the level of current in the ESD event can be approximated from the measured voltage by the sensor and from the *I–V* curve for the TVS.

Fig. 2 shows the high-level block diagrams of the external storage capacitor and the digital storage sensors. The digital storage sensor compares the voltage on the trace with a series of internal thresholds. A number of internal latches are set depending on whether the peak level exceeds the thresholds, thus performing a simple A/D conversion of the peak. The latches drive a current-controlled oscillator whose oscillation frequency is related to the peak level. The output of the oscillator is then driven off-chip, where it can create time-changing electric and magnetic fields that can be measured by an external probe.

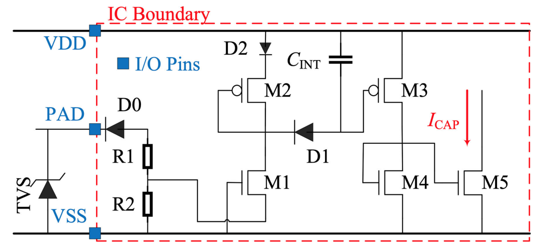

Fig. 3. Peak detector circuit for digital storage sensor.

In the external storage capacitor sensor design, a measure of the peak level of the transient event is stored on a large off-chip capacitor. This capacitor allows the level to be stored sufficiently long to allow the level to be determined by an external probe. A current proportional to the voltage on the capacitor drives a current-controlled oscillator similar to the other sensor. The sensor design for A/D-based design is explained first in the following paragraphs, followed by an explanation of the design using an external storage capacitor. The interconnectivity between the circuit blocks is represented by an arrow depicting current flow (I_{CAP}, I_0, and I_{Control}).

A. Peak Detector for Digital Storage Sensor

The negative peak detector circuit for the digital storage sensor is illustrated in Fig. 3. When the PAD voltage falls below VSS, the current is driven through diode D_0 and a positive gate-to-source voltage is created across NMOS M1. The size of the gate-to-source voltage is determined by resistors *R1* and *R2*, which are sized to prevent the oxide failure or snapback of M1 over the expected levels of transient events. If the gate-to-source voltage is larger than M1's threshold voltage, then a current will flow through M1 and PMOS M2, and a voltage roughly equivalent to the peak gate-to-source voltage of M2 will be stored on capacitor C_{INT}. Diode D_2 compensates for the voltage drop across D_1 to ensure the gate-to-source voltage of M2 and the voltage on C_{INT} is approximately equal. The voltage on C_{INT} creates the current I_{CAP}, which is sent to the A/D block of the sensor. C_{INT} stores a measure of the peak voltage for a sufficient time for the transient event to pass, for the on-die power supply to settle, and for the A/D to perform a conversion and to store the result.

B. Analog-to-Digital Converter

The A/D converter block is illustrated in Fig. 4. The current I_{CAP}, from Fig. 3, is fed as input to the circuit and mirrored to multiple current comparators, where I_{CAP} is compared with known current levels. The known currents are scaled versions of a reference current I_0 generated by an on-board threshold referenced source. Set-reset (SR) latch output D_0 is set if I_{CAP}

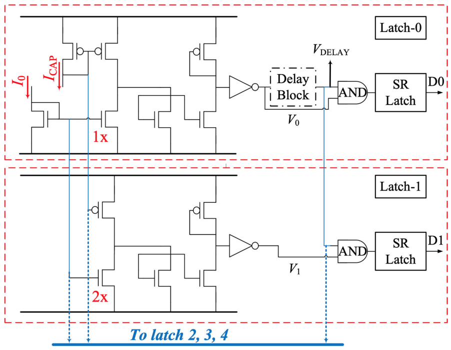

Fig. 4. A/D converter block. The peak detected level is digitized using current comparators, which trigger SR latches after a fixed delay.

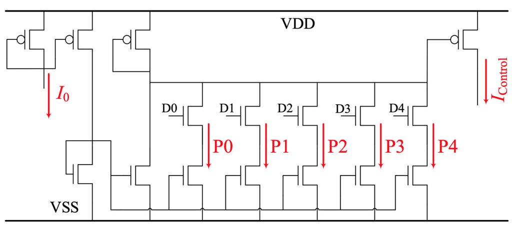

Fig. 5. D/A converter. Currents P_0–P_4 have magnitude I_0 when activated.

is larger than $1{*}I_0$. SR latch output D_1 is set if I_{CAP} is larger than $2{*}I_0$, and so on. There are five comparators corresponding to five discrete quantization levels of the detected peak voltage.

A delay block is implemented after the lowest level comparator to introduce a delay of approximately 600 ns before a latch can be triggered. This delay should provide sufficient time for the on-chip power supply to settle after an event to ensure that the accurate results are stored. Most transient events of interest are much shorter than 600 ns. Prior design experience suggests that the capacitor C_{INT} should hold its charge without significant leakage for several microseconds [9].

C. D/A Converter

The digital-to-analog (D/A) converter is shown in Fig. 5. The outputs D_0–D_4 of the A/D converter block turn ON NMOS FETs. The current drawn through these FETs is mirrored to the output I_{Control} such that

$$I_{\text{Control}} \approx I_0 + \sum I_0 \cdot D_i \tag{1}$$

where I_0 is the reference current from the on-die threshold referenced source and D_i are the SR latch outputs. During the idle state, I_{Control} is equal to the reference current I_0. I_{Control} grows linearly with the number of latches set. For example, if D_0 has been triggered, then I_{Control} is approximately $2I_0$, if D_0 and D_1 have been triggered, then I_{Control} is approximately $3I_0$, etc.

D. Current-Controlled Oscillator and Wireless Transmission

The current I_{Control} drives a current-controlled oscillator designed using five current starved inverters, as shown in Fig. 6 [13]. I_{Control} determines the drive current for each inverter. Larger currents lead to higher oscillation frequencies. The output of the oscillator is connected to a large driver, which is connected to an output pin.

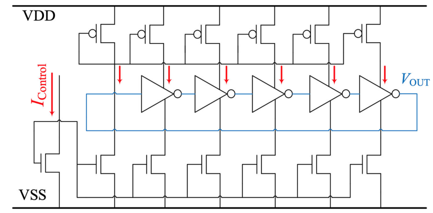

Fig. 6. Current-controlled oscillator.

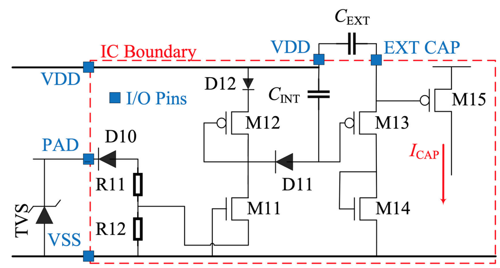

Fig. 7. Peak detector circuit for external-capacitor storage sensor.

This pin can be used to drive a large piece of floating metal to create an oscillating electric field or can be connected to a wire or trace connected to VSS to create a current loop and, thus, an oscillating magnetic field. It should be noted that only the frequency of oscillation of these fields is relevant, as the frequency is associated with the peak detected transient voltage. The magnitude of the oscillating field only has to be large enough to be detected.

E. Peak Detector for External-Capacitor-Based Sensor

The negative peak detector circuit for the external-capacitor-based sensor is illustrated in Fig. 7. This circuit is similar to the peak detector block in Fig. 3, but in this design, C_{INT} drives a source follower, which charges an external capacitor C_{EXT}. Capacitor C_{EXT} stores a measure of the peak transient event voltage and drives a current I_{CAP} proportional to the detected peak level.

F. Control Current for External-Capacitor-Based Design

The current I_{CAP} driven from the circuit in Fig. 7 is added with the reference current I_0, as illustrated in Fig. 8, so that $I_{\text{Control}} = I_{\text{CAP}} + I_0$. I_{Control} drives the current-controlled oscillator, as shown in Fig. 6. A larger peak event corresponds to a higher I_{CAP}, which in turn leads to a higher I_{Control} current. The larger currents lead to the higher oscillation frequencies. Unlike the A/D-based design, the control current and, thus, the output frequency of the capacitor-based design will vary continuously with the peak event level rather than taking only a set number of discrete values.

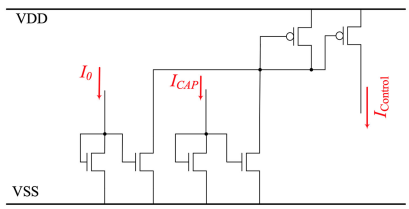

Fig. 8. Control current block for the external-capacitor-based design.

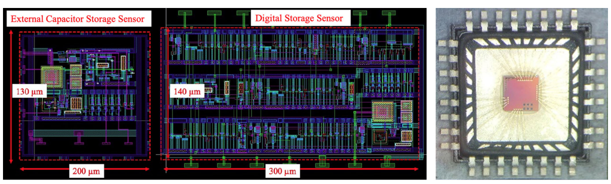

(a) (b)

Fig. 9. Implemented IC. (a) Layout. (b) Packaged IC.

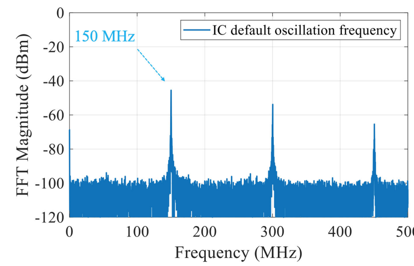

Fig. 10. Measured output from the A/D-based sensor in the idle state.

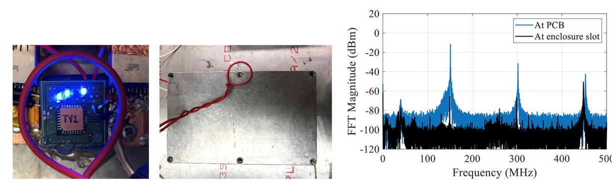

(a) (b) (c)

Fig. 11. Testing of the wireless transmission of the signal level. (a) Using a wire loop probe next to the PCB, without an enclosure. (b) Using a wire loop probe next to the enclosure lid slot, at a distance of about 5 cm away from the sensor PCB inside the enclosure. (c) Detected oscillator output.

G. Implementation of Sensors

The sensor circuits were implemented on a chip in 180 nm technology [11]. While the sensors were implemented in the same die, they had separate pins to allow each design to be evaluated individually. The sensors were mounted in a small thin quad flat package (TQFP) package, as illustrated in Fig. 9. The proof-of-concept sensors use four pins: VDD (+3.3 V), VSS, the sensor input pin (which is to be connected to the pin or trace of interest), and the oscillator output pin. The digital design also uses a reset pin to reset the SR latch states. This pin could reasonably be eliminated in a real application, for example, by using an internal timer to reset the SR latches after a given delay after a transient event.

III. Measurement-Based Validation

Evaluation boards were designed to test the sensors. The size of the board was 20 × 20 mm. The board includes a regulated power supply that provides a stable +3.3 V to the IC and protects the IC from drawing excessive current during a latch-up event or if the power pins are accidentally connected with the wrong polarity. For the A/D-based design, LEDs were provided to give a visual indication of the level of the sensed event (the state of D_0–D_5) up to level-2 and to reset the latches. For the external-capacitor-based design, a 100 nF capacitor was used to store the peak level of the event and circuitry was provided to allow the resetting of the external capacitor. A trace connected to the output pin of the sensors was run around the outside edge of the board, so the IC can drive a relatively large loop and generate relatively large magnetic fields. In a real implementation, this loop might be created with a thin wire or even by connecting the output pin directly to the VSS pin (thus, driving a small loop formed by the package lead frame).

A. Idle Sensor Output

Fig. 10 shows the signal measured by a nearby magnetic loop probe when the A/D-based sensor was in the idle state. The sensor generates oscillating magnetic fields at 150 MHz and its harmonics. The presence of the harmonics allows the sensor output to be detected either at the fundamental (i.e., 150 MHz) or at one of its harmonics if the fundamental is obscured by other emission sources. An R&S RTO1024 oscilloscope was used to measure the time-domain voltage and oscillation waveforms with a frequency bandwidth of 2 GHz and with a sampling rate of 10 GS/s.

B. Detection of the Oscillating Magnetic Fields

During actual use, the sensor might be placed in a product's metallic enclosure. A rough test was performed to demonstrate that the output of the sensor could be reasonably measured even in this case. First, a near-field loop probe was placed next to the printed circuit board (PCB) inside the enclosure, as illustrated in Fig. 11(a). Next, the loop was placed outside the enclosure with the lid shut but with a small gap between the lid and the rest of the enclosure, as illustrated in Fig. 11(b). As shown in Fig. 11(c), the magnitude of the signal measured using the loop probe was about −10 dBm at the PCB and was about −70 dBm just outside the enclosure.

Although the oscillation signal outside the enclosure was 60 dB lower than at the PCB, the signal frequency was still easily detected. Even outside the enclosure, the signal is 30 dB above the measurement noise floor, and an additional margin could be added using a smaller resolution bandwidth, low-noise amplifiers, or other techniques. This level is more than sufficient for determining the oscillator frequency. The larger signal strength at 450 MHz also illustrates why it could be useful to generate emissions at multiple frequencies. It is worth noting that the characteristics of the probe are not critical for this measurement since only the frequency of the oscillation is needed. When selecting a probe, its frequency range and loop

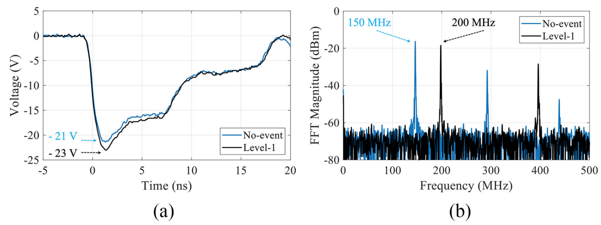

Fig. 12. Direct TLP injection results for digital storage sensor. (a) D_0 latch was triggered by a –23 V peak transient. (b) Sensor oscillator frequency corresponding to the peak level observed at the sensor detector pin.

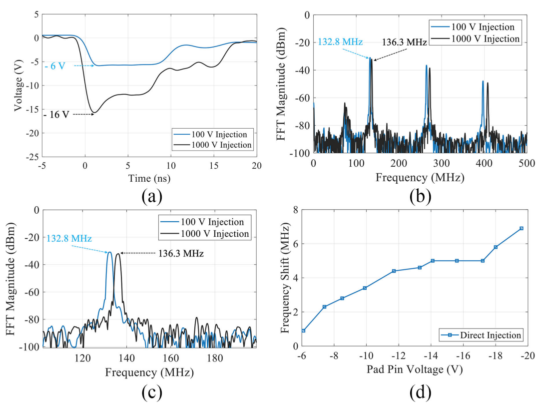

Fig. 13. Direct TLP injection results for the external-capacitor-based sensor. (a) Example waveforms at the detector pin. (b) Oscillator frequency output corresponding to the waveforms in (a). (c) Zoom-in of the frequency shift. (d) Change in oscillation frequency as a function of the peak detector pin voltage.

size should be considered. The placement of the loop probe may need to be adjusted to achieve an acceptable signal-to-noise ratio.

C. Sensor Characterization Using TLP and Direct Injection

To characterize the sensors, a TLP pulse [14] was directly applied to the sensor detector pin. A 2 ns rise time filter was used to filter the fast (<1 ns) rise time of the TLP pulse. Since the idle oscillator frequency depends on a threshold referenced source and the threshold voltage is expected to vary from one IC to another, the idle oscillator frequency is also expected to vary between the ICs. The precise idle oscillator frequency is unimportant, so long as one can measure it before testing starts. The level is determined from the change in frequency before and after a test.

1) A/D-Based Sensor: Fig. 12 shows the example transient waveforms that do and do not trigger the D_0 SR latch (a level-1 event) and the resulting sensor output. The peak voltage required to trigger the latch was about -23 V. The trigger of the D_0 latch was determined by the change in the output oscillator frequency. Here, the sensor oscillation frequency changed from 150 to about 200 MHz when D_0 was triggered.

2) External-Capacitor-Based Sensor: Fig. 13 shows the example waveforms that trigger the sensor and the resulting sensor output. Unlike the digital storage sensor, the output of this sensor will change for even very small changes in the peak understress

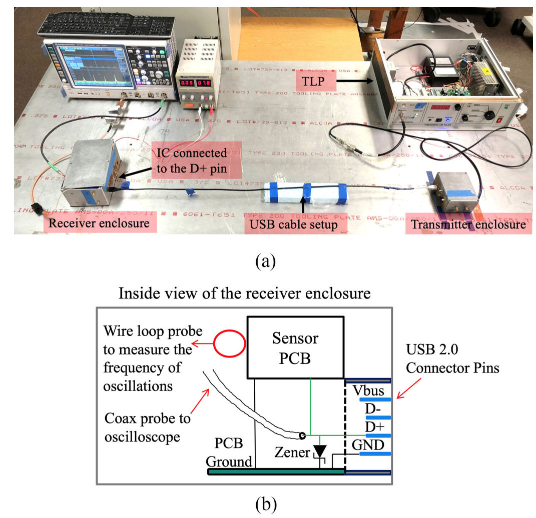

Fig. 14. Testing of a cable-connected discharge event. (a) Overall measurement setup. (b) Connection of the sensor to the D+ USB signal and the enclosure.

voltage. It is not required to reach a minimum level before a change occurs. Here, the sensor oscillation was about 132 MHz for a -6 V event and 136 MHz for a -16 V event. Fig. 13(d) shows the output frequency shift from the baseline (about 131 MHz) as a function of the peak event level. This plot was created by measuring multiple output waveforms while increasing the TLP injection voltage from 100 to 1000 V. The output oscillation frequency varies roughly linearly with the peak event level as expected.

D. Peak Detection in a USB Cable Discharge Event Setup

After initial validation that the sensor worked as expected, the sensors were further tested under a realistic system-level ESD scenario. An ESD discharge to a USB-connected device with an unshielded USB cable is known to generate relatively high-stress levels at the USB input [15]. The setup in Fig. 14(a) represents a USB-connected device, where an ESD discharge to one device leads to a cable-guided discharge event at the USB I/O pin of the other device. Here, a TLP was used as an injection source rather than an ESD gun to improve repeatability between the tests. The TLP pulse was applied between the "transmitter" shield and the reference plane. An unshielded USB cable was used to connect the transmitter to the receiver. The sensor was placed inside the receiver and connected between the D+ USB connector pin and the receiver enclosure. The transmitter was raised slightly above the return plane, so it was not shorted to the plane. The receiver was shorted directly to the return plane.

The simplified diagram of the connections inside the receiver is shown in Fig. 14(b). A coax probe was connected to the D+ pin to monitor the peak voltage generated by the TLP event at this pin. This coax probe was connected to the 50-Ω oscilloscope channel. To prevent instrument damage, 20-dB ESD high-voltage attenuators with a frequency bandwidth of 3.5 GHz were connected between the coax cable and the oscilloscope. A zener diode was placed from the D+ pin to the enclosure to

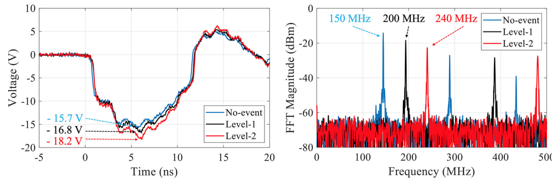

(a) (b)

Fig. 15. Detection of a cable-connected discharge event using the A/D-based sensor. (a) Transient voltage waveforms at the sensor detector pin. (b) Sensor oscillator outputs corresponding to the peak level observed at the sensor detector pin.

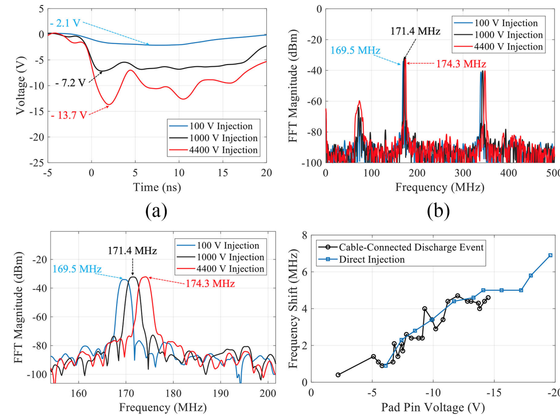

(a) (b) (c) (d)

Fig. 16. Detection of a cable-connected discharge event using an external-capacitor-based sensor. (a) Transient voltage waveforms at the sensor detector pin. (b) Sensor oscillator outputs corresponding to the peak level observed at the sensor detector pin. (c) Zoom-in of the frequency shift. (d) Change in oscillation frequency as a function of the peak detector pin voltage.

help protect the sensor in case of a large transient event. The sensor detector pins were connected to the D+ pin of the USB connector at the receiver, thus allowing the sensor to detect the voltage at the D+ pin and wirelessly transmit the peak level to an external probe. A wire loop probe was placed on the top of the sensor PCB to detect the wirelessly transmitted signal, as indicated in Fig. 14(b).

1) A/D-Based Sensor: The measured waveform on the receiver's D+ pin during the TLP event is shown in Fig. 15(a). The D_0 latch was triggered when a peak negative voltage of about -16.8 V appeared on the sensor input pin. For voltages less than -16.8 V, the sensor remained in the "idle" state. For an event of about -18.2 V, both the D_0 and D_1 latches were triggered, as indicated by the change in output frequency and the number of LEDs lit. Before the application of the TLP pulse, the sensor's oscillation frequency was about 150 MHz and all three LEDs were lit. When the D_0 latch was triggered (level-1 event), the oscillation frequency changed to about 200 MHz and the D_0 LED turned OFF. When both the D_0 and D_1 latches were triggered (level-2 event), the frequency changed to about 240 MHz and the D_0 and D_1 LEDs turned OFF. The results in Fig. 15(b) were calculated in a short period after the transient event had passed, so only show the "final" value of the oscillation and not the oscillation frequency before or during the event. The sensor was reset between each subsequent test.

2) External-Capacitor-Based Sensor: The results of testing the external-capacitor-based sensor are shown in Fig. 16. Fig. 16(a) shows the waveforms at the receiver's D+ pin for three example events. As the injection level was increased from 100 V to 1000 V and to 4400 V, the output frequency changed to roughly 170, 171 and 174 MHz, respectively. A plot of the change in the sensor output frequency as a function of the peak event is shown in Fig. 16(d). The change in frequency observed with the transient event is highly consistent between the direct injection measurements and the cable-guided event, as indicated in the plot.

IV. Discussion

For these proof-of-concept designs, only negative-level sensing was implemented. The results demonstrate that the sensing circuits work relatively well. Extending the designs to detect positive events, using a mirrored version of the detectors built with PFETs, should be relatively straightforward.

Process variation caused significant changes in the oscillation frequency from one design to another. For instance, the default oscillation frequency was about 100, 150, and 160 MHz for three different ICs implementing the A/D-based sensor. This variation is not surprising, given that the oscillation frequency depends directly on the threshold voltage, which can easily vary by $\pm$20–30%. The exact oscillation frequency is not important—only that one can detect the change in frequency when it occurs. More concerning, however, is that this variation caused a change in the trigger voltages used by the A/D converter. Ideally, the trigger voltage would be independent of process variation. For future designs, a reference that is less sensitive to process variation should be used, such as a bandgap reference. A bandgap reference could not be used here because of the lack of a standard bipolar junction transistor model in the CMOS process, which is used to build the test circuit.

A similar shift in the base oscillation frequency of the external-capacitor-based sensor was observed between the direct injection test setup (a base frequency of about 131 MHz) and the USB test setup (about 169 MHz). The reason for the change in the base oscillation frequency is unclear and is under investigation. The change in frequency observed with the transient event, however, is highly consistent between the measurements, as indicated in Fig. 16(d). This result further emphasizes that the baseline oscillation frequency is not critical because it is the change in the output frequency, which is used to indicate the peak understress voltage during the transient event. The variation in the initial oscillation frequency is expected in this design. The value of the transient peak voltage is best determined by measuring the output frequency just before and after the event, and considering the shift in frequency between the two.

The tests of the A/D-based sensor were performed up to the point that the D_0 and D_1 latches were triggered (a level-1 and level-2 event), although the IC is capable of testing up to five levels. The sensor performed much as expected for these first two levels. A default oscillation was observed until a suitable sized event occurred, at which time the output oscillation increased in the frequency relative to the size of the event.

The sensors were tested using TLP pulses with 2 ns rise time and pulsewidth less than 10 ns. Additional testing using an ESD generator and the TLP waveforms with varying rise times and pulsewidths are needed to fully understand the limits of the sensor design. Larger events were not tested at this time due to the limited number of sensor test ICs available and the fear that the ICs might be destroyed during the testing process.

The oscillating magnetic fields were easily observed in the test setups used here. Even weaker fields could easily be observed with modest changes to the measurement setup. The level of the observed fields, however, may vary dramatically depending on the size of the loop used to generate the field or the shielding effectiveness of the metal enclosure. It would not be surprising if a much smaller transmitting loop was used in the final application, perhaps only a few square millimeter in area. Additional testing is needed to demonstrate if these fields could be reasonably detected, although the strong initial results are promising. Using the sensor to generate oscillating electric fields has not yet been tested. One advantage of using an electric-field source is that a small insulated wire could easily be snaked from the sensor through the electronic product to a place where it was near a connector or gap in an enclosure and where the output signal might make its way outside a well-shielded enclosure more efficiently.

For the digital storage sensor, the voltage required to trigger a level-1 detection was different in the direct injection test (-23 V, Fig. 12) than in the cable-guided event (-16.8 V, Fig. 15). The cable-guided event created an input waveform with much slower rise time and no "overshoot" compared with the waveform seen at the sensor pin during the direct injection. We expect that the signal seen by the sensor on-die, however, is a low-pass filtered version of the signal seen at the IC pin due to the package inductance, the series resistance of the sensor, and the on-die capacitance of the ESD protection and of resistors $R1$, $R2$, and FET M1 (see Fig. 3). This low-pass filtered version of the direct-injected signal in Fig. 12 likely looks much closer to the cable-guided waveform, as shown in Fig. 15. Further study is needed to verify this hypothesis. Future designs should take this effect into account to maximize their ability to detect short-duration peaks.

Both sensor designs have their advantages and disadvantages. The primary advantage of the A/D-based design is that it can hold the reading almost indefinitely until the sensor is repowered or reset. Distinguishing between the output levels is easy and unambiguous, without requiring any real calibration, but one can distinguish between only a few discrete levels. Since the output frequency of the external-capacitor-based design varies directly with the peak level of the event, it provides the possibility of a much greater resolution than the A/D-based design. It also can detect much lower level events than the A/D-based design. Even very small negative understress voltages would cause a change in the external-capacitor-based sensor's output oscillation frequency. The understress voltage did not have to reach a minimum trigger level to cause a change in the output as for the A/D-based design. The external-capacitor-based sensor also allowed a gradual change in the output frequency with peak event level, allowing the possibility of more accurately detecting the level of the event. On the downside, however, the external capacitor was only capable of holding the output oscillation frequency steady for several microseconds before the capacitor voltage began to drop along with the oscillation frequency. This limitation required that the output oscillation frequency be carefully monitored during testing to accurately determine the peak voltage. For the A/D-based design, the output oscillation frequency remained steady until the sensor was reset. The hold time of the external capacitor might be increased by making the capacitor larger but will require a larger drive circuit (M3 and M4 in Fig. 7) to ensure that the external capacitor C_{EXT} may be fully charged before the internal capacitor C_{INT} discharges significantly.

V. Conclusion

Both sensors show significant promise for the debugging of ESD issues, particularly those related to soft failures where there may be no "smoking gun" left to indicate which component or trace allowed the failure to occur. The sensors may allow the electromagnetic compatibility engineer to probe traces or pins during an ESD test without modifying the enclosure (e.g., to allow measurement cables to run in and out) and without changing the product layout. If the sensor was made sufficiently small, for example, made using an unpackaged die or very small packaging option, such as a chip-scale package, it might be used in highly dense product designs, such as a cell phone.

The measurements provided by the sensor could significantly reduce the time required to debug the cause of ESD issues and could provide direct feedback as to the impact of design changes intended to reduce the transient levels seen by sensitive components.

References

[1] Electromagnetic Compatibility (EMC)—Part 4-2: Electrostatic Discharge Immunity Test, IEC Standard 61000-4-2, Ed. 2.0, 2008.

[2] W. B. Kuhn, R. J. Eatinger, and S. A. Melton, "ESD detection circuit and associated metal fuse investigations in CMOS processes," *IEEE Trans. Device Mater. Rel.*, vol. 14, no. 1, pp. 146–153, Mar. 2014.

[3] N. Thomson, C. Reiman, Y. Xiu, and E. Rosenbaum, "On-chip monitors of supply noise generated by system-level ESD," in *Proc. 39th Elect. Overstress/Electrostatic Discharge Symp.*, Sep. 2017, pp. 1–10.

[4] M.-D. Ker, C.-C. Yen, and P.-C. Shih, "On-chip transient detection circuit for system-level ESD protection in CMOS integrated circuits to meet electromagnetic compatibility regulation," *IEEE Trans. Electromagn. Compat.*, vol. 50, no. 1, pp. 13–21, Feb. 2008.

[5] H.-C. Chow and Z.-H. Hor, "A high performance peak detector sample and hold circuit for detecting power supply noise," in *Proc. IEEE Asia Pac. Conf. Circuits Syst.*, Nov. 2008, pp. 672–675.

[6] W. Lee *et al.*, "An on-die oscilloscope for system-level ESD noise monitoring," in *Proc. IEEE Int. Symp. Electromagn. Compat., Signal/Power Integrity*, 2019, pp. 156–160.

[7] N. Jack and E. Rosenbaum, "Voltage monitor circuit for ESD diagnosis," in *Proc. Elect. Overstress/Electrostatic Discharge Symp.*, Sep. 2011, pp. 1–9.

[8] A. Patnaik *et al.*, "An on-chip detector of transient stress events," *IEEE Trans. Electromagn. Compat.*, vol. 60, no. 4, pp. 1053–1060, Aug. 2018.

[9] A. Patnaik *et al.*, "On-chip sensors to measure level of transient events," in *Proc. 39th Elect. Overstress/Electrostatic Discharge Symp.*, Sep. 2017, pp. 8A.1-1–8A.1-10.

[10] A. Patnaik, R. Hua, and D. Pommerenke, "Characterizing ESD stress currents in human wearable devices," in *Proc. 39th Elect. Overstress/Electrostatic Discharge Symp.*, Sep. 2017, pp. 3A.3-1–3A.3-6.

[11] A Patnaik, S. Marathe, S. Liu, D. Pommerenke, and D. G. Beetner, "A transient event sensor for efficient system-level ESD testing," *IEEE Trans. Electromagn. Compat.*, vol. 60, no. 5, pp. 1231–1239, Oct. 2018.

[12] S. Marathe, A. Patnaik, K. Ghosh, J. Kim, D. Pommerenke, and D. G. Beetner, "Experimental validation of an intergrated circuit transient electromagnetic event sensor," in *Proc. IEEE Int. Symp. Electromagn. Compat., Signal/Power Integrity*, 2019, pp. 161–166.

[13] R. J. Baker, *CMOS: Circuit Design, Layout, and Simulation*, 3rd ed. New York, NY, USA: Wiley, 2011.

[14] "TLP-1000 series transmission line pulse generator." 2019. [Online]. Available: https://www.esdemc.com/products/system-level-esd-test/tlp-1000-series-transmission-line-pulse-generator/

[15] S. Marathe, P. Wei, S. Ze, L. Guan, and D. Pommerenke, " Scenarios of ESD discharges to USB connectors," in *Proc. 39th Elect. Overstress/Electrostatic Discharge Symp.*, Sep. 2017, pp. 1–6.

Shubhankar Marathe (Member, IEEE) received the B.E. degree in electronics and telecommunication from the University of Mumbai, Mumbai, India, in 2013, and the M.S. and Ph.D. degrees in electrical engineering from the Electromagnetic Compatibility (EMC) Laboratory, Missouri University of Science and Technology, Rolla, MO, USA, in 2017 and 2019, respectively.

In 2019, he joined Amazon Lab126, Sunnyvale, CA, USA, as an Electrostatic Discharge (ESD) System Design Engineer. His research interests include near-field scanning, ESD, EMC measurements, and signal integrity.

Dr. Marathe was a recipient of the 2018 IEEE EMC Society President's Memorial Award at the Joint IEEE EMC and APEMC Symposium, Singapore, 2018.

Abhishek Patnaik (Member, IEEE) received the B.E. degree from the Institute of Technical Education and Research, Bhubaneswar, India, in 2010, and the M.S. and Ph.D. degrees in 2015 and 2018, respectively, from the Electromagnetic Compatibility (EMC) Laboratory, Missouri University of Science and Technology, Rolla, MO, USA, all in electrical engineering.

He is currently pursuing his career as an RF Desense Engineer. His current research interests include on-chip electrostatic discharge design, RF circuit design, RF immunity, EMC testing, grounding, and shielding techniques to improve EMC.

Rui Mi received the B.S. degree from the Missouri University of Science and Technology, Rolla, MO, USA, in 2019 where he is currently working toward the M.S. degree with the Electromagnetic Compatibility Laboratory, both in electrical engineering.

His current research interests include RF circuits, instrumentation, and electromagnetic interference measurement and design.

Kaustav Ghosh (Member, IEEE) received the B.E. degree in electronics and telecommunication engineering from Nagpur University, Nagpur, India, in 2012, and the master's degree in electrical engineering from the Missouri University of Science and Technology, Rolla, MA, USA, in 2018.

Since March 2016, he has been a Graduate Research Assistant with the Electromagnetic Compatibility (EMC) Lab, Missouri University of Science and Technology. He is currently an EMC Design Engineer with Juniper Networks, Sunnyvale, CA, USA. His current research interests include numerical and experimental study of electromagnetic interference (EMI) problems at a system level and board level, power supply EMC, analysis of EMI emission issues, and different EMI mitigation techniques.

Mr. Ghosh is a member of the IEEE EMC society.

Jingook Kim (Senior Member, IEEE) received the B.S., M.S., and Ph.D. degrees in electrical engineering from the Korea Advanced Institute of Science and Technology, Daejon, Korea, in 2000, 2002, and 2006, respectively.

From 2006 to 2008, he was a Senior Engineer with the DRAM design team in the Memory Division of Samsung Electronics, Hwasung, Korea. From January 2009 to July 2011, he was a Postdoctoral Fellow with Electromagnetic Compatibility (EMC) Laboratory, Missouri University of Science and Technology, Rolla, MA, USA. In July 2011, he joined the Ulsan National Institute of Science and Technology, Ulsan, Korea, where he is currently an Associate Professor. His current research interests include high-speed I/O circuits design, 3D-IC, EMC, electrostatic discharge, and RF interference.

David Pommerenke (Fellow, IEEE) received the Diploma and the Ph.D. degree from the Berlin Institute of Technology, Berlin, Germany, in 1996.

His current research interests include electromagnetic compatibility (EMC), RF interoperability, system-level electrostatic discharge, electronics, numerical simulations, and EMC measurement methods and instrumentations. After working with Hewlett Packard for five years, he joined the EMC Laboratory, Missouri University of Science and Technology, in 2001, and changed to CTO with ESDEMC Technology LLC, in 2019. Since 2020, he has been a Professor with EMC and RF Coexistence Laboratory, Graz University of Technology, Graz, Austria. He has co-authored more than 200 journal papers and is an inventor on 13 patents.

Prof. Pommerenke is an Associate Editor for the TEMC.

Daryl G. Beetner (Senior Member, IEEE) received the B.S. degree from Southern Illinois University, Edwardsville, IL, USA, in 1990, and the M.S. and D.Sc. degrees from Washington University, St. Louis, MO, USA, in 1994 and 1997, respectively, all in electrical engineering.

He is currently a Professor and the Chair of electrical and computer engineering with the Missouri University of Science and Technology (formerly the University of Missouri-Rolla), Rolla, MO, USA, where he conducts research with the Electromagnetic Compatibility Laboratory on electromagnetic immunity and emissions from the integrated circuit to the system level.